

Published in final edited form as:

*Nat Struct Mol Biol.* 2016 September ; 23(9): 786–793. doi:10.1038/nsmb.3266.

## Skp is a multivalent chaperone of outer membrane proteins

Bob Schiffrin<sup>#1,2</sup>, Antonio N. Calabrese<sup>#1,2</sup>, Paul W. A. Devine<sup>1,2</sup>, Sarah A. Harris<sup>1,3</sup>, Alison E. Ashcroft<sup>1,2</sup>, David J. Brockwell<sup>1,2</sup>, and Sheena E. Radford<sup>1,2</sup>

<sup>1</sup>Astbury Centre for Structural Molecular Biology

<sup>2</sup>School of Molecular and Cellular Biology, University of Leeds, Leeds, UK

<sup>3</sup>School of Physics and Astronomy, University of Leeds, Leeds, UK

# These authors contributed equally to this work.

### Abstract

The trimeric chaperone Skp sequesters outer membrane proteins (OMPs) within a hydrophobic cage, preventing their aggregation during transport across the periplasm in Gram negative bacteria. Here, we study the interaction between *Escherichia coli* Skp and five OMPs of varying size. Investigations of the kinetics of OMP folding reveal that greater Skp:OMP ratios are required to prevent the folding of 16-stranded OMPs compared with their 8-stranded counterparts. Ion mobility spectrometry-mass spectrometry (IMS-MS) data, computer modelling and molecular dynamics simulations provide evidence that 10- to 16-stranded OMPs are encapsulated within an expanded Skp substrate cage. For OMPs which cannot be fully accommodated in the expanded cavity, sequestration is achieved by binding of an additional Skp trimer. The results suggest a new mechanism for Skp chaperone activity involving coordination of multiple copies of Skp to protect a single substrate from aggregation.

---

$\beta$ -barrel outer membrane proteins (OMPs) perform numerous essential and diverse functions in the outer membrane (OM) of Gram negative bacteria. After synthesis in the cytoplasm, OMPs are translocated across the inner membrane, and then must traverse the periplasm before reaching the OM, where the  $\beta$ -barrel Assembly Machinery (BAM) complex folds and inserts them<sup>1–5</sup>. While the periplasmic chaperones Skp and SurA are considered the major OMP chaperones in *E. coli*, a network of folding factors is involved in OMP assembly, including Trigger Factor and SecB in the cytoplasm, and FkpA and DegP in the periplasm<sup>1,6,7</sup>. Periplasmic chaperones act without an external energy source (unlike many

---

Users may view, print, copy, and download text and data-mine the content in such documents, for the purposes of academic research, subject always to the full Conditions of use:[http://www.nature.com/authors/editorial\\_policies/license.html#terms](http://www.nature.com/authors/editorial_policies/license.html#terms)

Correspondence should be addressed to S.E.R. (s.e.radford@leeds.ac.uk), D.J.B. (d.j.brockwell@leeds.ac.uk) or A.E.A. (a.e.ashcroft@leeds.ac.uk).

#### Author contributions

B.S. and A.N.C. contributed equally to this work. B.S. designed and performed the kinetic experiments, computer modelling and molecular dynamics simulations. A.N.C. designed and performed the mass-spectrometry and cross-linking experiments. P.W.A.D. designed and performed *in vacuo* apo-Skp simulations. S.A.H. assisted and supervised the molecular dynamics simulations. A.E.A., D.J.B. and S.E.R. conceived, designed and supervised the research. All authors contributed to discussion and were involved in editing the final manuscript.

#### Competing Financial Interests Statement

The authors declare no competing financial interests.

of the Hsp chaperones<sup>8</sup>), as the periplasm is devoid of ATP<sup>5</sup>, and bind and release their substrates by mechanisms that are not well understood<sup>7</sup>.

The holdase chaperone Skp protects OMPs against misfolding and aggregation during their transit between the inner and outer membranes<sup>9–11</sup>. Skp has broad substrate specificity<sup>12</sup>, with reported affinities for its substrates in the low nanomolar range<sup>13,14</sup>. Skp is a functional homotrimer (referred to herein as Skp) with a ‘jellyfish’-like architecture (Fig. 1a)<sup>10,11</sup>, consisting of three  $\alpha$ -helical ‘legs’ that extend 60 Å away from the ‘body’ domain; a 9-stranded  $\beta$ -barrel which mediates trimerisation<sup>10,11</sup>. The three subunits of Skp form a hydrophobic cavity inside which OMP clients are bound<sup>9,12,15,16</sup>, with previous studies suggesting a 1:1 stoichiometry for all Skp:OMP complexes<sup>13,17,18</sup>. These 1:1 stoichiometries have been proposed using tryptophan fluorescence (Skp complexes formed with tOmpA (19 kDa)<sup>13</sup>, NalP (32 kDa)<sup>13</sup>, OmpG (33 kDa)<sup>13</sup>, OmpA (35 kDa)<sup>13,17</sup> and BamA (89 kDa)<sup>13</sup>), by NMR (OmpX (16 kDa) and tOmpA (19 kDa)<sup>15</sup>) and by fluorescence correlation spectroscopy (OmpC (38 kDa)<sup>18</sup>). The Skp hydrophobic cavity has been estimated to be able to accommodate folded proteins of ~25 kDa<sup>10</sup>, but many OMPs known to interact with Skp are considerably larger (e.g. the 22-stranded BtuB and the 26-stranded LptD are 66 kDa and 87 kDa, respectively)<sup>12</sup>. This raises fundamental questions about the structural alterations that must occur for Skp to accommodate its larger substrates.

To investigate the mechanism by which Skp sequesters OMPs of different sizes, we used kinetic studies of OMP folding complemented with electrospray ionization-ion mobility spectrometry-mass spectrometry (ESI-IMS-MS) analyses to examine the interactions of Skp with five diverse OMPs: 1) tOmpA, the 8-stranded transmembrane domain of OmpA<sup>19</sup>; 2) PagP, an 8-stranded acyl transferase enzyme<sup>20</sup>; 3) OmpT, a 10-stranded protease<sup>21</sup>; 4) OmpF, a 16-stranded trimeric porin<sup>22</sup>; and 5) tBamA, the 16-stranded transmembrane domain of the BamA OMP insertase<sup>23</sup> (Fig. 1b-f, Supplementary Table 1). We find that the concentration of Skp required to prevent OMP insertion into  $di_{C11:0}PC$  liposomes increases as the mass of client OMP increases, suggesting that the sequestration mechanism of Skp is altered for larger OMP clients. ESI-IMS-MS and computer modelling were used to examine the conformations of Skp:OMP complexes and provided evidence that the core of Skp expands to accommodate the larger OMPs, with the largest clients requiring the formation of 2:1 Skp:OMP assemblies to completely sequester the polypeptide chain. Combined, the results provide a new understanding of how Skp is able to bind, chaperone and release substrates that vary dramatically in size, with expansion of the binding cage and/or formation of multivalent complexes allowing the chaperone to adapt to the demands of its clients.

## Results

### Different Skp:OMP ratios are required to inhibit OMP folding

To assess the effects of Skp on the folding and membrane insertion of OMPs of varied size, folding assays were performed by diluting unfolded protein stock solutions (in 8 M urea) 33-fold into buffer containing ~100 nm diameter synthetic  $di_{C11:0}PC$  liposomes. The increase in tryptophan fluorescence associated with folding was then measured as a function of time. Maintaining a low protein concentration (0.4  $\mu$ M) and a high lipid:protein ratio (3200:1)

enables folding to be monitored in a low final concentration of urea (0.24 M) without interference from aggregation. This approach enables real time measurements of folding that are complementary to SDS-PAGE based studies which have been used to provide information about the fraction of folded (SDS-resistant) protein present at a particular time<sup>24–26</sup>.

To verify that the OMPs selected for study are able to fold into  $d\text{I}_{\text{C}11:0}\text{PC}$  liposomes and/or interact with Skp under the experimental conditions selected, fluorescence emission spectra of each OMP were measured in 8 M or 0.24 M urea in the absence of liposomes (in the latter case with and without a two-fold molar excess of Skp). These spectra were then compared with those of membrane inserted (folded) OMP obtained at the end point of the folding reaction (Fig. 2a-d). Spectra of tOmpA, PagP, OmpF and tBamA folded into liposomes show a characteristic blue-shift in  $\lambda_{\text{max}}$  and increase in fluorescence intensity compared with spectra of the unfolded proteins in 8 M urea, indicating that a substantial fraction of all four OMPs fold successfully into the liposomes employed. In the presence of Skp, the spectra of tOmpA, OmpF and tBamA show decreases in  $\lambda_{\text{max}}$  and/or intensity compared with spectra of these OMPs in buffer alone, demonstrating that these unfolded OMPs interact with Skp. For PagP no change in fluorescence is observed in the presence of Skp, although these proteins do interact, as shown in previous work<sup>27</sup>.

The effect of Skp on OMP folding kinetics was next investigated. In the absence of Skp, the OMPs fold with either single or double exponential kinetics (Fig. 2a-d), allowing extraction of the folding rate constants ( $k_1$  and  $k_2$ ) (Fig. 2a-d, Supplementary Table 2). To verify that the transients obtained reflect membrane insertion and folding, assays were performed in the absence of lipids (Supplementary Fig. 1). A folding transient is observed only for OmpT in the absence of lipid (Supplementary Fig. 1e), presumably reflecting folding of the large extracellular region of OmpT which contains three tryptophan residues (Supplementary Fig. 1f). For all other OMPs, no change in fluorescence was observed over time in the absence of lipid, indicating the formation of a stable soluble form, as previously reported<sup>13,27</sup>. The folding kinetics of OMPs that had been pre-incubated with Skp at molar ratios ranging from 1:1 to 4:1 (chaperone:client) (where Skp concentrations are in trimer equivalents, see Online Methods) were then measured by adding the pre-formed complexes to  $d\text{I}_{\text{C}11:0}\text{PC}$  liposomes and monitoring OMP folding by fluorescence spectroscopy (Fig. 2a-d, Supplementary Fig. 2). The results show that at a substrate concentration of 0.4  $\mu\text{M}$ , a 2-fold molar excess of Skp is sufficient to prevent tOmpA and PagP folding into liposomes (Fig. 2a, b, Supplementary Fig. 2a, b). We have previously shown that while incubation of Skp with PagP at a 2:1 ratio prevents OMP folding over a 2 h timescale, overnight incubation with liposomes allows OMP release and folding to equivalent yields as in the absence of Skp<sup>27</sup>. For both of the 8-stranded OMPs tOmpA and PagP, a 1:1 Skp:OMP ratio retards folding, while a 2:1 ratio prevents folding over the timescale of the experiment. By contrast, pre-incubation of OmpF and tBamA with a 2-fold excess of Skp decreases the folding rate, but does not prevent folding (Fig. 2c, d, Supplementary Fig. 2c, d). However, pre-incubation with a 4-fold excess of Skp inhibits folding of these larger proteins over the timescale of the experiment (Fig. 2c, d, Supplementary Fig. 2c, d). The results suggest, therefore, that complete sequestration of larger OMP barrels requires the binding of more than one copy of Skp.

## Stoichiometries of Skp:OMP assemblies studied by ESI-MS

To gain insights into the architectures of Skp:OMP assemblies, we exploited ESI-MS coupled with IMS to analyze different Skp:OMP complexes within multicomponent mixtures. Skp assemblies with tOmpA, PagP, OmpT, OmpF and tBamA were prepared, and mass spectra acquired using instrumental conditions that allow non-covalent interactions to be retained *in vacuo* (termed non-covalent or “native” MS)<sup>28–30</sup> (see Online Methods) (Fig. 3, Supplementary Fig. 3a-f, Supplementary Table 3). The results show that all five Skp:OMP assemblies are sufficiently stable to survive the ESI process and be transferred into the gas phase for analysis.

Several reports have suggested that Skp binds unfolded OMPs ranging from 16-89 kDa (8-16  $\beta$ -strands in the native state) with a 1:1 stoichiometry<sup>13,15,17,18</sup>. By contrast, the mass spectra shown in Fig. 3 reveal that the stoichiometry of these assemblies is dependent on the size of the OMP client, consistent with the kinetic traces described above. Thus, tOmpA and PagP (8-stranded OMPs) bind only one Skp, whilst the larger OMPs, OmpT, OmpF and tBamA (10- and 16-stranded OMPs) bind up to two copies of Skp. Peaks corresponding to monomeric Skp subunits were also observed ( $m/z \sim 2000$ ) (Fig. 3), indicating either that some dissociation of the assembly is occurring in-source, and/or reflecting the population of monomeric subunits in solution<sup>31,32</sup>. Interestingly, a 2:1 assembly is the predominant complex observed in the spectrum for the largest 16-stranded OMP studied, tBamA, despite being formed by mixing Skp with tBamA at a 1:1 molar ratio (Fig. 3f). A 2:1 Skp:OMP assembly was also observed for full-length BamA (Supplementary Fig. 4a,b). To confirm that the Skp:OMP stoichiometry observed using ESI-MS reflects the stoichiometry in solution, we performed chemical cross-linking with bis(sulfosuccinimidyl)suberate (BS3), followed by SDS-PAGE analysis of Skp pre-incubated with full-length OmpA or full-length BamA. In the cross-linked Skp:OmpA samples, a 1:1 assembly was observed (Supplementary Fig. 5a-d) whereas in the Skp:BamA samples a band consistent with a complex with a 2:1 stoichiometry (but no 1:1 Skp:BamA complex) was observed (Supplementary Fig. 5e-g).

## Insights into Skp:OMP complex structure from ESI-IMS-MS

How Skp binds its OMP clients of larger size was next analyzed using ESI-IMS-MS. IMS measures the mobility of ions through an inert gas-filled chamber under the influence of a weak electric field, with the drift time (mobility) of an ion in this environment dependent on its mass, size and charge<sup>28,33</sup>. Here, we used travelling wave IMS-MS<sup>28,33</sup>, for which calibration of the measured drift time data can be performed to obtain rotationally averaged collision cross-sections (CCSs), to provide insight into the conformations of Skp and the Skp:OMP assemblies. IMS data were acquired for all of the assemblies studied (Fig. 4a-f, Supplementary Fig. 3a-f), and compared with known structures where available, or with models of the Skp:OMP complexes for which there are no high resolution structural data.

Fig. 4a-f displays the CCS distributions of the observed ions originating from Skp and 1:1 Skp:OMP complexes, normalized to spectral intensity (a representative dataset is shown from three independent experiments). The modal CCSs are also plotted as a function of charge state in Fig. 4g (Supplementary Table 4). Interestingly, the CCSs of the Skp ions (Fig.

4g) are smaller than expected based on the published Skp crystal structure (the modal CCS at the lowest observed charge state, which is least affected by Coulombic repulsion<sup>34</sup>, was 37.9 nm<sup>2</sup>, approximately 25 % lower than the expected value of 45.7 nm<sup>2</sup> derived from the crystal structure (Fig. 4g)). Molecular dynamics simulations (Supplementary Fig. 6, **Supplementary Data Sets 1 and 2**) revealed that the assembly collapses in the gas phase, resulting in a structure with CCS of 37.3 ± 1.9 nm<sup>2</sup> (Fig. 4g).

Binding of Skp to the 8-stranded tOmpA and PagP (Fig. 4g) results in ions with increased CCS compared with Skp alone. The CCSs of the ions observed (45.6 nm<sup>2</sup> and 45.8 nm<sup>2</sup> for Skp:tOmpA and Skp:PagP, respectively, at the lowest observed charge state) compare favorably with the CCS predicted from the crystal structure of Skp alone (45.7 nm<sup>2</sup>), supporting the notion that these assemblies are specific complexes in which the OMP is located within the central Skp cavity, preventing collapse of the chaperone in the gas phase<sup>15,16</sup>. Consistent with this, the Skp:OMP complexes sample a narrower conformational ensemble compared with Skp alone, measured by the width at half height of the mobility peaks observed (Fig. 4a-c). Complexation with tOmpA and PagP thus packs the hydrophobic cavity of Skp resulting in a narrower conformational ensemble, consistent with previous data<sup>15</sup>.

Interestingly, the 1:1 Skp:OMP assemblies of the larger OMPs studied (OmpT, OmpF and tBamA) (Fig. 4g) have increased CCSs (51.4-54.2 nm<sup>2</sup>) compared with the Skp:tOmpA and Skp:PagP assemblies (~46 nm<sup>2</sup>). These data, together with mismatch between the volume of Skp's cavity and the volume likely to be occupied by larger OMP clients in the 'fluid globule' state<sup>15</sup>, suggest that the central cavity expands in size to encapsulate these species, consistent with recent SANS data<sup>35</sup>. However, the kinetic data (Fig. 2c,d) indicate that Skp expansion is insufficient to fully sequester these larger OMPs in a 1:1 complex.

Plotting the increase in CCS as a function of molecular weight for Skp and all complexes (Fig. 4h), including 2:1 Skp:OMP assemblies (Supplementary Fig. 3g), reveals that the data fit to a globular model, irrespective of client size. The complexes exhibit an effective gas phase density of 0.33 Da.Å<sup>-3</sup>, similar to values reported for other protein complexes<sup>33</sup>, and consistent with recent calculations of the CCSs of globular proteins in the PDB <sup>36</sup>.

### Modelling of larger OMPs in complex with two copies of Skp

Models for the architecture of Skp in complex with OmpT, tBamA or OmpF were next generated to determine how Skp and a partially folded OMP may interact. Four different models were constructed. As a starting point, encapsulated tOmpA was modelled as a sphere with a radius of 20 Å (Fig. 5a) which has a volume of 33,500 Å<sup>3</sup>, consistent with previous estimates<sup>10,15</sup>. We assumed that the amino acid density for non-native OMPs bound to Skp is independent of the mass of the OMP studied, consistent with the MS data presented above. Therefore, to model a 16-stranded OMP, we assumed a spherical volume of ~67,000 Å<sup>3</sup> giving a radius of ~25 Å, and generated a Skp model with its three subunits surrounding a sphere of this size (Fig. 5b). The theoretical CCS of the resulting structure (50.4 nm<sup>2</sup>) (Fig. 4g) is in good agreement with the measured CCS values for 1:1 Skp:OmpT, Skp:OmpF and Skp:tBamA complexes (51.4, 51.8 and 54.2 nm<sup>2</sup>, respectively) (Fig. 4g, Supplementary

Table 4). The results suggest, therefore, that 1:1 Skp:OMP complexes with larger OMPs, involve an expanded Skp cavity.

Next, we generated models of the 2:1 Skp:OMP complexes, theorizing that Skp could arrange in a side-by-side configuration, in either a parallel or antiparallel arrangement (Fig. 5c,d), with the OMP represented by a capsule. The theoretical CCSs of these assemblies were determined to be 79.1 and 78.2 nm<sup>2</sup>, respectively (Fig. 4g). Alternatively, we considered a model in which the OMP substrate (represented by a sphere with a radius of ~25 Å) may be encapsulated by two interlocked copies of Skp (Fig. 5e), which results in a complex with a theoretical CCS of 73.5 nm<sup>2</sup> (Fig. 4g). All three values are in good agreement with the measured CCS values for 2:1 Skp:OmpT, Skp:OmpF and Skp:tBamA complexes (71.7, 71.2 and 72.8 nm<sup>2</sup>, respectively) (Fig. 4g, Supplementary Table 4).

### Molecular dynamics simulations to model Skp:OMP complexes

To model the Skp:OMP complexes further and aid their visualization, we performed a series of molecular dynamics simulations. A simulation of apo-Skp in explicit solvent over 100 ns demonstrated that the individual subunits are highly dynamic and flexible. Each subunit undergoes a transition to an ‘open’ state, in which subunit helices splay from the central axis, resulting in an expanded central cavity, consistent with previous MD studies<sup>18,35</sup> (Supplementary Fig. 7a-c, **Supplementary Data Sets 1 and 3**, Supplementary Video 1). The average radius of gyration ( $R_g$ ) of Skp from the simulation (31.5 Å) is in good agreement with published SANS data (~33 Å)<sup>35</sup>. This  $R_g$  is ~10 % higher than that predicted from the crystal structure, indicating that dynamic motions of the Skp subunits observed in the simulation likely reflect those in solution. In the two Skp crystal structures solved to date<sup>10,11</sup>, the lower section of one of the subunits is unresolved, indicating flexibility, and the angles with which the Skp subunits extend away from the ‘body’ domain are different for each of the subunits in the two structures<sup>10,11</sup>. The subunits in the crystal structure of the heterohexameric eukaryotic chaperone prefoldin (Fig. 5f) also make different angles with respect to the multimerisation domain, which has also been suggested to indicate conformational flexibility that may be functionally relevant<sup>37</sup>.

Next, we generated models of tOmpA (8-stranded) and tBamA (16-stranded) alone in an unfolded, extended conformation, and simulated their behavior in solvent (mimicking the situation in which OMPs are diluted from 8 M urea). In each case, the OMPs collapse rapidly to an approximately globular form (Supplementary Fig. 7d,e, Supplementary Video 2). A model of the 1:1 Skp:tOmpA complex was then generated by placing the collapsed tOmpA structure within the cavity of Skp in an ‘open’ conformation from the simulation of apo-Skp (Supplementary Fig. 7b) and relaxing the resulting structure *in vacuo*. In the simulation, the subunits of Skp collapse rapidly around the tOmpA substrate resulting in a structure with a CCS value ( $43.7 \pm 1.2$  nm<sup>2</sup>) in excellent agreement with that measured by ESI-IMS-MS ( $45.6 \pm 0.1$  nm<sup>2</sup>), suggesting that, at least in the gas phase, Skp “clamps” around the substrate (Fig. 6a,b, Supplementary Video 3). A model for the gas-phase 2:1 Skp:tBamA complex was created by placing the collapsed tBamA structure in the hydrophobic cavity formed by two copies of Skp in their ‘open’ conformations. A side-by-side parallel orientation (Fig. 6c) was chosen based on the striking resemblance of this

model to the structure the eukaryotic prefoldin chaperone<sup>37</sup> (Fig. 5f). The size of the collapsed tBamA model clearly exceeds the maximal dimensions of the cavity of a single Skp observed in an ‘open’ conformation (Fig. 6c). Simulation of the 2:1 Skp:tBamA complex *in vacuo* showed that the Skp subunits also rapidly “clamp” around the tBamA substrate creating a complex with a CCS value ( $74.4 \pm 1.4 \text{ nm}^2$ ) again in good agreement with the IMS data ( $72.8 \pm 0.2 \text{ nm}^2$ ) (Fig. 6d, Supplementary Video 4). Thus, the CCS data obtained from both experiment and simulation (Supplementary Table 5) are consistent with a model in which multivalent Skp binding is necessary to sequester OMPs that exceed the dimensions of the Skp cavity.

To provide evidence that a similar “clamping” motion of Skp around its OMP substrates could occur in solution, we performed analogous MD simulations of Skp:tOmpA and 2:1 Skp:tBamA complexes in explicit solvent. In these simulations Skp subunits are also observed wrapping around their OMP substrates (Fig. 7a,b, Supplementary Videos 5,6), with ‘clamping’ movements similar to those observed in the gas-phase simulations (Fig. 6). The complexes formed are stable over 100 ns (Fig. 7c,d) and have larger calculated CCS values ( $56.5 \pm 0.3 \text{ nm}^2$  and  $101.2 \pm 6.0 \text{ nm}^2$  for Skp:tOmpA and 2:1 Skp:tBamA, respectively) than those following gas-phase simulation ( $43.7 \pm 1.2 \text{ nm}^2$  and  $74.4 \pm 1.4 \text{ nm}^2$  for Skp-tOmpA and 2:1 Skp-tBamA, respectively). These data are consistent with a model in which the subunits of Skp are dynamic, resulting in expansion of the hydrophobic cavity that allows entry of substrates of varying sizes, prior to the Skp subunits ‘wrapping’ around the sequestered client to protect it from aggregation until folding into the bilayer can take place.

## Discussion

Major advances in the understanding of the cascade of molecular chaperones and folding catalysts involved in OMP biogenesis have been made in recent years, yet the molecular details of how OMPs are bound by molecular chaperones, transported across the periplasm and assembled into the outer membrane, without using the energy of ATP binding/hydrolysis, remain unclear<sup>1,7,23</sup>. Here, we have provided new insights into how Skp is able to chaperone its broad array of OMP clients, including substrates which are too large to be accommodated within its hydrophobic cavity. We have shown that Skp utilizes subunit dynamics to expand the size of its client binding cavity and have demonstrated that Skp can function as a multivalent chaperone in order to sequester and prevent aggregation of its larger OMP clients. Further, we have used ESI-IMS-MS to gain structural insight into the 1:1 and 2:1 Skp:OMP complexes we have identified. Using kinetic refolding and ESI-IMS-MS data, combined with MD simulations, we present models consistent with the experimental results in which Skp sequesters larger OMPs by binding in a multivalent arrangement (side-by-side parallel or anti-parallel, and/or via an interlocking structure) (Fig. 5c-e). The parallel side-by-side model (Fig. 5c) bears a striking resemblance to the structure of the non-homologous chaperone prefoldin (Fig. 5f)<sup>37</sup>. The precise orientation(s) of Skp molecules in these multivalent complexes will require more information to resolve, for example using cross-linking experiments followed by MS/MS. Nonetheless, the biochemical, MS and MD results presented indicate that the ability of Skp to chaperone OMPs ranging from 35-43 kDa in size requires both subunit dynamics and its ability to function as a multivalent chaperone.

Skp has been shown *in vivo* to interact with much larger substrates than those investigated here (19-43 kDa), including BtuB (66 kDa), FhuA (79 kDa) and LptD (87 kDa) which form  $\beta$ -barrels composed of 22, 22, and 26  $\beta$ -strands, respectively<sup>12,38</sup>. It is likely these proteins also form multivalent complexes with Skp and indeed recent data on the interaction between Skp and FhuA is consistent with a greater than 1:1 Skp:OMP stoichiometry<sup>39</sup>.

The results presented have implications for our understanding of how OMPs are chaperoned by Skp in the periplasm, including the mechanisms of substrate binding and release. Our atomistic MD trajectories of apo-Skp show that it exists in a wide range of open conformations with large differences in the area of the cavity entrance formed between the tips of its three subunits. Such conformational flexibility has been implicated in the mechanisms of other ATP-independent chaperones<sup>40,41</sup>. We propose that in rescuing aggregation-prone proteins<sup>6</sup> Skp could be thought of as analogous to a pair of 'calipers', sampling open conformations prior to capture of its client, allowing it to adjust the volume of its central cavity. In this model once the substrate has entered the Skp cavity, the Skp subunits 'clamp down' to protect the exposed hydrophobic surfaces of the protein, in a mechanism similar to those of other chaperones such as Trigger Factor or Hsp90<sup>42</sup>. For substrates which are too large to be accommodated within the Skp substrate cavity, additional copies of Skp recognize and engulf sections of the substrate not already encapsulated. *In vivo* cross-linking evidence suggests that Skp can interact with OMPs as they emerge from the SecYEG translocon<sup>43</sup>. Thus it is possible that during translocation of larger OMPs, the substrate is fed directly into the cavity of Skp and the chaperone's maximum binding capacity would then be reached before the complete polypeptide chain is translocated. Subsequent polypeptide chain emerging from the translocon could then be bound by a second or more Skp(s), ensuring sequestration of the entire polypeptide sequence so that periplasmic aggregation is prevented.

Recent equilibrium sedimentation experiments of Skp in the absence of substrate have demonstrated a dynamic equilibrium between folded subunit monomers and trimers at physiological concentrations<sup>32</sup>. Therefore, a possible alternative *in vivo* pathway to Skp-OMP complex formation may involve sequential binding of monomer subunits to OMP substrates, with Skp trimerization linked to (and indeed driven by) substrate binding. Sandlin *et al.* raise the possibility that more diverse species of Skp could form around an unfolded OMP<sup>32</sup>. However, for the complexes studied here only Skp-OMP complexes containing monomeric Skp subunits in multiples of three are observed (Fig. 3), suggesting either that the trimeric unit is the OMP binding species, or that complexes of other composition are unstable in the gas-phase.

It has been proposed that transient exposure of the C-terminal OMP targeting sequence ( $\beta$ -signal)<sup>44,45</sup>, and its recognition by the BAM complex<sup>46</sup>, triggers substrate release from Skp<sup>15</sup>. The space between Skp subunits ( $\sim 25$  Å in the crystal structure<sup>10</sup>) and/or the inherent dynamics of the complex may facilitate the transient solvent-exposure of regions of the OMP substrate, permitting  $\beta$ -signal recognition. Consistent with this, the presence of BamA in liposomes relieves the folding inhibition of OmpA by Skp *in vitro*<sup>47</sup>. It is interesting to note that in all 2:1 Skp:OMP models proposed here there remains a substantial distance ( $> 20$  Å) between the Skp subunits which would permit exposure of sections of the substrate



polypeptide required for BAM signalling and/or membrane insertion. The release of the OMP from Skp is likely to be driven by the increased thermodynamic stability of the folded OMP relative to the chaperone-bound state<sup>48</sup>, and for OMPs that are bound to more than one Skp, it is possible that individual copies of Skp are released sequentially in a process driven by the free energy of OMP folding.

Chaperones utilize two general strategies to protect substrates from misfolding and aggregation. In the first, substrates are chaperoned by sequential binding and release of exposed hydrophobic surfaces along an extended polypeptide chain. This ‘beads on a string’ model is typified by chaperones such as the Hsp70s and Trigger Factor<sup>8,49</sup>. Alternatively, aberrant interactions may be prevented by sequestration of the substrate from the cellular environment within an enclosed space, as is the case for the ‘cage-like’ chaperonins such as GroEL/ES and TriC<sup>8,49</sup>. The data presented here suggest that Skp operates with a ‘hybrid’ mechanism, employing both of these strategies to bind and encapsulate its OMP clients, thereby preventing their aggregation and facilitating their delivery to the OM wherein folding can successfully occur.

## Online Methods

### Cloning of OmpF, tBamA and OmpT

A codon optimized synthetic gene (Eurofins, Germany) of the mature sequence of OmpF (residues 23-362) was cloned into pET11a (Novagen, UK) between the NdeI (5′) and BamHI (3′) restriction sites. To create the tBamA construct, residues 425-810 of BamA were amplified by PCR, using plasmid BamAB-pETDUET-1 (kindly donated by Dr Susan Buchanan (NIH, USA)) as the template, and the resultant product then ligated into pET11a as described above. The OmpT mature sequence (residues 21-217) was amplified by PCR from *E. coli* XL1-blue cells to include an N-terminal 6xHis-tag and TEV protease cleavage site (MH<sub>6</sub>ENLYFQG-OmpT), and subsequently cloned into the pET11a vector as described above. The plasmids for tOmpA, PagP, OmpA and BamA encoding the mature OMP sequences were kindly provided by Dr Karen Fleming (John Hopkins University, USA)<sup>25</sup>.

### Expression and purification of PagP, tOmpA, OmpF, tBamA, OmpA and BamA

The relevant plasmid was transformed into BL21[DE3] cells (Stratagene, UK) and the appropriate OMP was expressed and purified as previously described<sup>27</sup>. Protein concentrations were determined spectrophotometrically using molar extinction coefficients at 280 nm of 82,390, 46,870, 54,210, 101,315, 52,955 and 140,040 M<sup>-1</sup> cm<sup>-1</sup> for PagP, tOmpA, OmpF, tBamA, OmpA and BamA, respectively.

### Expression and purification of OmpT

Expression and purification for OmpT was carried out as previously described<sup>54</sup>. Protein concentration was determined spectrophotometrically using a molar extinction coefficient at 280 nm of 79,760 M<sup>-1</sup> cm<sup>-1</sup>.

### Expression and purification of Skp

The pET21b plasmid, containing the full-length Skp gene, including the N-terminal signal sequence, was transformed into BL21[DE3] cells (Stratagene, UK). Cells were grown in LB medium containing 100 µg/mL carbenicillin at 27 °C with shaking (200 rpm) until the culture reached an OD<sub>600</sub> of ~0.6 (after ~6 h). Cultures were induced with 25 µM IPTG, expressed overnight, and harvested by continuous centrifugation at 15000 rpm (Heraeus Contifuge, Rotor 8575, Thermo Fisher Scientific, UK). The cell pellet was resuspended in 50 mM Tris-HCl, 5 mM EDTA, 50 mM NaCl, pH 7.5 at 4 °C with gentle agitation for ~48 h. 1 mg/mL polymyxin B sulphate was added to the resuspended cells, and then incubated for 1 h at 4 °C with gentle agitation. Spheroplasts were sedimented by centrifugation (12 000 g, 20 min 4 °C) and the supernatant dialyzed against 20 mM Tris-HCl, 100 mM NaCl, pH 8.0 (Buffer A) overnight at 4 °C. The periplasmic extract was filtered (0.4 µm syringe filter, Sartorius, UK) and loaded onto a HiTrapQ (5 mL) anion exchange column (GE Healthcare, UK). The flow through from this column was loaded onto a HiTrap SP (5 mL) cation exchange column (GE Healthcare, UK) equilibrated with Buffer A. The column was washed with 5 column volumes of Buffer A and eluted with a gradient (0-100 %) of 20 mM Tris-HCl, 750 mM NaCl, pH 8.0 (Buffer B). Peak fractions were dialysed against 20 mM Tris-HCl, pH 8.0 and concentrated to ~50 µM (trimer) using Vivaspin 20 (5 kDa MWCO) concentrators (Sartorius, UK). Aliquots were snap-frozen in liquid nitrogen and stored at -80 °C. Protein concentrations were determined using a bicinchoninic acid (BCA) assay (Thermo Fisher Scientific, UK), according to the manufacturer's instructions.

### Expression and purification of His-tagged Skp

His-tagged Skp was expressed and purified using a protocol adapted from Burmann *et al.*<sup>15</sup>. The pET28b plasmid, containing the Skp gene with an N-terminal 6xHis-tag and thrombin cleavage site, was transformed into BL21[DE3]pLysS cells (Stratagene, UK). Cells were grown in LB medium containing 30 µg/mL kanamycin at 37 °C with shaking (200 rpm) until the culture reached an OD<sub>600</sub> of ~0.6. The temperature was then lowered to 20 °C and expression induced with 0.4 mM IPTG. Following overnight expression (~18 h) cells were harvested by centrifugation, resuspended in 25 mM Tris-HCl, pH 7.2, 150 mM NaCl, 20 mM imidazole, containing a cocktail of EDTA-free protease inhibitors (Roche), and lysed using a cell disrupter (Constant Cell Disruption Systems, UK). Following centrifugation to remove cell debris (20 mins, 4 °C, 39000 g), the lysate was applied to 5 mL HisTrap columns (GE Healthcare) and washed with 25 mM Tris-HCl, pH 7.2, 150 mM NaCl, 20 mM imidazole. His-tagged Skp was denatured on-column with 25 mM Tris-HCl, 6 M Gdn-HCl, pH 7.2, and eluted with a 0-500 mM imidazole gradient over 50 mL in 25 mM Tris-HCl, 6 M Gdn-HCl, pH 7.2. Fractions containing Skp were pooled and the protein refolded by dialysis against 25 mM Tris-HCl, pH 7.2, 150 mM NaCl. Refolded His-tagged Skp was concentrated to ~50 µM (trimer) using Vivaspin 20 (5 kDa MWCO) concentrators (Sartorius, UK), aliquoted, snap-frozen in liquid nitrogen and stored at -80 °C. Protein concentrations were determined using a bicinchoninic acid (BCA) assay (Thermo Fisher Scientific, UK), according to the manufacturer's instructions.

## Preparation of liposomes

1,2-diundecanoyl-*sn*-glycero-3-phosphocholine (*d*C<sub>11:0</sub>PC) (DUPC) lipids were purchased from Avanti Polar Lipids (Alabama, USA). DUPC was obtained as a powder, dissolved in a 80:20 chloroform:methanol mixture at 25 mg/mL, and stored at -20 °C until use.

Appropriate volumes were transferred to glass test tubes and an even lipid film was created by drying with a gentle stream of nitrogen while being shaken moderately in a 42 °C water bath. Lipid films were further dried in a vacuum desiccator for >3 h, followed by resuspension in 50 mM glycine-NaOH, pH 9.5 to a concentration of 40 mM. Resuspended lipids were vortexed briefly and allowed to stand for 30 min. After vortexing again, lipids were subjected to 5 freeze-thaw cycles using liquid nitrogen. Large Unilamellar Vesicles (LUVs) (100 nm) were prepared by extruding the lipid suspension 11 times through a 0.1 µm polycarbonate membrane (Nuclepore, New Jersey, USA) using a mini extruder (Avanti Polar Lipids, Alabama, USA). Liposomes were stored at 4 °C and used within 48 h of preparation.

## Kinetic folding assays

Kinetic measurements were carried out using a Quantum Master Fluorimeter (Photon Technology International, UK) controlled by FelixGX software v4.3. For each experiment, four separate samples were run in a four cell changer maintained at 25 °C by a peltier-controlled temperature unit. Tryptophan fluorescence of samples was excited at a wavelength of 295 nm, and fluorescence emission was monitored at 335 nm. 295 nm rather than 280 nm was chosen as the excitation wavelength as this minimizes the fluorescence intensity contribution from Skp, which contains tyrosine but no tryptophan residues. The excitation slit widths were set to 0.4-0.6 nm and the emission slit widths were set to 5 nm. The high emission:excitation slit width ratio was important to minimize photobleaching on the experimental time-scale. OMPs were buffer exchanged from 25 mM Tris-HCl, 6 M Gdn-HCl, pH 8.0 into 50 mM glycine-NaOH, 8 M urea, pH 9.5 using Zeba spin desalting columns (Thermo Scientific, UK) and diluted to 80 µM. OMP folding reactions in the absence of Skp were initiated by diluting OMPs manually from this 80 µM unfolded protein stock in 8 M urea to a final concentration of 0.4 µM protein and 0.24 M urea in the presence of 1.28 mM DUPC liposomes (a lipid:protein molar ratio (LPR) of 3200:1), in 50 mM glycine-NaOH, pH 9.5. Stable folding of Skp in 0.24 M urea was verified by CD (data not shown). The final volume for each sample was 500 µL. For Skp-OMP experiments, OMPs were pre-incubated with Skp for approximately 1 min prior to addition of liposomes. OMPs were diluted and mixed from an 80 µM stock in 8 M urea to a final concentration of 2.4 µM, in the presence the appropriate molar ratio of Skp, in 0.24 M urea, 50 mM glycine-NaOH, pH 9.5 (no lipids). This Skp-OMP stock was then further diluted 6x in presence of 1.28 mM DUPC in 0.24 M urea, 50 mM glycine-NaOH, pH 9.5 to begin the assay. The final volume for each sample was 540 µL. At the concentrations of Skp utilized here, Skp has been shown to be in a dynamic equilibrium between folded monomer subunits and trimers<sup>32</sup>. All Skp concentrations referred to here are trimer equivalents. For each experiment with a particular liposome batch, four samples were measured concurrently. A minimum of three replicates were globally fitted using IgorPro 6.0 (Wavemetrics, Oregon, USA) to extract rate constant(s), forcing the fits to share the same rate constant(s). Transients were fitted either to a single exponential function:

$$y=A_1 \cdot e^{-k_1 t}+c$$

or to a double exponential function:

$$y=(A_1 \cdot e^{-k_1 t})+(A_2 \cdot e^{-k_2 t})+c$$

Where  $k_1$  and  $k_2$  are rate constants,  $A_1$  and  $A_2$  are their associated amplitudes, and  $c$  is a constant. Transients were fitted to a double exponential function if a satisfactory fit was not obtained to a single exponential function as judged by inspection of residuals. Experiments were performed for each condition using three separate liposome batches, and reported errors are the standard deviation of rate constants between liposome batches.

### Fluorescence emission spectra

Fluorescence emission spectra were acquired on the same instrument as the kinetic assays (above). Each spectrum was recorded from 305 nm to 400 nm in 1 nm increments, using an excitation wavelength of 295 nm. All spectra were acquired at 25 °C and all samples contained 50 mM glycine-NaOH, pH 9.5, in a sample volume of 500  $\mu$ L. OMPs from an 80  $\mu$ M stock in 8 M urea were diluted to a final concentration of 0.4  $\mu$ M in the presence of a 2-fold molar excess of Skp in 0.24 M urea, 8 M urea, or buffer alone in 0.24 M urea. Folded samples were prepared by dilution of an 80  $\mu$ M OMP stock to 0.4  $\mu$ M in the presence of 1.28 mM DUPC liposomes (molar LPR 3200:1) in 0.24 M urea and incubated at 25 °C for ~1.5 h prior to acquisition of the fluorescence emission spectra.

### Mass Spectrometry

Skp:OMP complexes were prepared by rapid dilution of the denatured OMP (400  $\mu$ M in 8 M urea, 50 mM glycine-NaOH, pH 9.5) to a final concentration of 5  $\mu$ M into a solution of Skp (5  $\mu$ M in 50 mM glycine-NaOH, pH 9.5). The samples were then buffer exchanged into 200 mM ammonium acetate, pH 10 using Zeba spin desalting columns (Thermo Scientific, UK) immediately prior to MS analysis. nanoESI-IMS-MS spectra were acquired using a Synapt HDMS mass spectrometer (Waters Corporation, UK) using platinum/gold-plated borosilicate capillaries prepared in-house. Typical instrument parameters include: capillary voltage 1.2-1.6 kV, cone voltage 40 V, trap collision voltage 6 V, transfer collision voltage 10 V, trap DC bias 20 V, backing pressure 4.5 mBar, IMS gas pressure 0.5 mBar, travelling wave height 7 V, travelling wave velocity 250  $\text{ms}^{-1}$ . Data were processed using MassLynx v4.1, Driftscope 2.5 (Waters Corporation, UK) and Massign55. CCSs were estimated by a calibration approach<sup>28,33,56</sup> using arrival time data for ions with known CCSs ( $\beta$ -lactoglobulin A, avidin, concanavilin A and yeast alcohol dehydrogenase, all Sigma Aldrich, UK). Estimated modal CCSs are shown as mean  $\pm$  standard deviation of three independent experiments. Theoretical CCSs for globular proteins with a given effective gas phase density were calculated according to published methods<sup>57</sup>.

### Chemical cross-linking and SDS-PAGE analysis.

Samples for chemical cross-linking were prepared by rapid dilution of the urea denatured OMP into a Skp solution (in 20 mM HEPES pH 7.5, 150 mM NaCl) at 4 °C, so that the final concentrations of Skp and OMPs were 20  $\mu$ M in a final concentration of 0.24 M urea. Samples were mixed for 2 min and centrifuged (20 min, 13,000 *g*, 4 °C) to remove aggregated material. The supernatant was removed and bis(sulfosuccinimidyl)suberate (BS3) (Thermo Scientific, UK) was added at a 50-fold molar excess over the Skp concentration. Samples were incubated at room temperature for 30 min, before the addition of 250 mM glycine pH 9.5. Samples were analyzed by SDS-PAGE and the gels stained with Coomassie Blue (InstantBlue, Expedeon, UK), or the proteins transferred to a PVDF membrane and immunoblotted with an anti-His-HRP conjugated antibody (catalogue no. 15165, Thermo Scientific, UK).

Gel bands were excised, cut into 1 mm<sup>3</sup> pieces, destained with 30 % ethanol and washed with 50 % acetonitrile in 25 mM ammonium bicarbonate (10 min). The gel pieces were then dehydrated with acetonitrile (5 min), and the residual volatile solvent removed by evaporation. They were then rehydrated with a solution of trypsin (Promega, UK) (20 ng  $\mu$ L<sup>-1</sup> in 25 mM ammonium bicarbonate) and incubated at 37 °C for 18 hours. Peptides were recovered by incubating the gel pieces with 60 % acetonitrile/5 % formic acid (x 3), and the samples were then concentrated.

Peptides were analysed by means of data-dependent LC-MS/MS on a nanoAcquity LC system interfaced to a Synapt G2-Si HDMS mass spectrometer (Waters Ltd., Wilmslow, Manchester, UK). Peptides (1  $\mu$ L) were injected onto an Acquity M-Class C18, 75  $\mu$ m x 150 mm column (Waters Ltd., Wilmslow, Manchester, UK) and then separated by gradient elution of 1-50 % solvent B (0.1 % (v/v) formic acid in acetonitrile) in solvent A (0.1 % (v/v) formic acid in water) over 60 min at 0.3  $\mu$ L min<sup>-1</sup>. Mass calibration was performed by a separate injection of aqueous sodium iodide at a concentration of 2  $\mu$ g/ $\mu$ L. [Glu1]-Fibrinopeptide B was infused as a lock mass calibrant. Data acquisition was achieved using data dependent analysis with a one second MS scan over an *m/z* range of 350-2000 being followed by four 0.5 second MS/MS scans taken of the four most intense ions in the MS spectrum. Data processing was performed using PEAKS Studio 7 (Bioinformatics Solutions, Ontario, Canada).

### Modelling of Skp-OMP complexes

All modelling was performed with the PyMOL Molecular Graphics System (v1.7rc1). To generate models of the Skp:OMP complexes, the missing residues in chains B and C of the Skp crystal structure (PDB: 1U2M10) were modelled from chain A. For the Skp:tOmpA/PagP model (Fig. 5a) the OMP was modelled as a sphere of radius 20 Å with its origin positioned at the geometric center between the  $\alpha$ -carbon atoms of residue 50 of each Skp chain. For the Skp:OMP model with expanded Skp subunits (Fig. 5b), each chain was positioned around a sphere of radius 25 Å representing the larger OMP. The flexible tips of each subunit (residues 51-101) were modelled hinged slightly inwards to wrap around the substrate. The side-by-side parallel and antiparallel 2:1 Skp:OMP models (Fig. 5c,d) were created by duplication of the Skp:tOmpA/PagP model (Fig. 5a) and appropriate rotation and

translation. The interlocking trimer 2:1 Skp:OMP model (Fig. 5e) was generated by duplication of the Skp model with expanded subunits (Fig. 5b) and appropriate rotation and translation of the duplicated Skp. Theoretical CCS values were generated using the calibrated trajectory method implemented in the software IMPACT36.

## Molecular Dynamics Simulations

Molecular dynamics (MD) simulations were prepared using the AmberTools 14 suite of programs, and performed using AMBER and the ff14SB forcefield58. To simulate apo-Skp in water, a Skp model was first generated from the Skp crystal structure (PDB: 1U2M10) with the residues absent in chains B and C modelled from chain A. Following addition of hydrogen atoms using xleap, Skp was placed in a TIP3P water box with a 10.0 Å cutoff and the system neutralized with a total of 15 Cl<sup>-</sup> ions. The system was equilibrated by performing an initial energy minimization, followed by 80 ps of restrained MD during which the system was heated to 300 K with gradual releasing of restraints. This was followed by an unrestrained MD simulation of 100 ns.

Simulations of the collapse of the extended chains of tOmpA and tBamA were carried out using a Generalized Born/Solvent Accessible surface area (GB/SA) implicit solvent model59,60. Use of an implicit solvent model speeds up exploration of conformational space by at least an order of magnitude due to the neglect of frictional forces from collisions with water molecules61, leading to rapid adoption of a collapsed configuration from the initially linear structure (Supplementary Fig. 7d, e, Supplementary Video 2). The polypeptide starting structures were generated in xleap and, after initial energy minimization, were simulated for 3 ns. The starting models for the simulation of Skp-tOmpA and Skp<sub>2</sub>-tBamA *in vacuo* were created in PyMol by positioning OMPs, after simulated collapse, within the cavity of Skp trimer structures in an 'open' conformation taken from the explicit solvent apo-Skp simulation. All simulations except apo-Skp in explicit water were performed in triplicate. Each *in vacuo* simulation of Skp-tOmpA and 2:1 Skp:tBamA was performed using a starting OMP structure from a different simulation. *In vacuo* simulations of apo-Skp were performed using three different starting structures selected from the simulation of apo-Skp in explicit water. For all *in vacuo* simulations the system was equilibrated by performing an initial energy minimization, followed by eight steps of restrained MD during which the system was heated to 300 K with gradual releasing of restraints. This was followed by an unrestrained MD simulation of 100 ns.

To simulate the 1:1 Skp:tOmpA and 2:1 Skp:tBamA complexes in solution, starting models were generated as detailed above for the *in vacuo* simulations. The Skp:OMP complexes were placed in a TIP3P water box with a 10.0 Å cutoff and the system neutralized with a total of 10 Cl<sup>-</sup> ions (1:1 Skp:tOmpA) or 12 Cl<sup>-</sup> ions (2:1 Skp:tBamA). The systems were equilibrated by performing an initial energy minimization, followed by 80 ps of restrained MD during which the system was heated to 300 K with gradual releasing of restraints. This was followed by an unrestrained MD simulation of 100 ns. For each complex simulations were repeated in triplicate.

For comparison with IMS-MS data, theoretical collision cross-sections (CCSs) of final structures at the end of simulations were calculated using the trajectory method and the

software IMPACT36. CCS values for all structures following *in vacuo* simulations were obtained after 100 ns of unrestrained simulation. CCS values for tOmpA and tBamA in implicit solvent were obtained after 3 ns of unrestrained simulation. The integration time-step was 2 fs and atomic positions were saved every 500 steps (1 ps). The software VMD was used to compute backbone root mean square deviation (RMSD) and to render videos of the simulations. Analysis of radius of gyration changes over trajectories were carried out with ptraj.

## Supplementary Material

Refer to Web version on PubMed Central for supplementary material.

## Acknowledgements

The plasmids containing the mature sequences of tOmpA, PagP, OmpA and BamA were kindly provided by K. Fleming (John Hopkins University, USA)<sup>25</sup>. Plasmid pET21b (Novagen) containing the Skp gene was a gift from J. Bardwell (University of Michigan, USA). We also thank S. Hiller (University of Basel, Switzerland) for kindly providing the His-tagged Skp construct<sup>15</sup>, and S. Buchanan (NIH, USA) for the gift of plasmid BamAB-pETDUET-1. We thank T. Watkinson (University of Leeds, UK) for expression and purification of OmpT, and M. Jackson (University of Leeds, UK) for help with western blots, and are also grateful for the assistance and advice of L. M. McMorran (University of Leeds, UK) in the early stages of this work. This work was supported by Biotechnology and Biological Sciences Research Council (BBSRC) grants BB/J014443/1 (B.S.), BB/K000659/1 (A.N.C), and BB/J011819/1 (P.W.A.D.). Funding from the European Research Council under the European Union's Seventh Framework Programme grant FP7.2007-2013/grant agreement number 322408 (A.E.A., D.J.B. and S.E.R) is also acknowledged. The Waters Synapt G1 and G2-Si mass spectrometers were purchased with funding from the BBSRC (BB/E012558/1 and BB/M012573/1, respectively). This project made use of time on the ARC2 supercomputer facility at the University of Leeds, and time on ARCHER granted via the UK High-End Computing Consortium for Biomolecular Simulation, HECBioSim ([www.hecbiosim.ac.uk](http://www.hecbiosim.ac.uk)), supported by the EPSRC (grant no. EP/L000253/1).

## References

1. McMorran LM, Brockwell DJ, Radford SE. Mechanistic studies of the biogenesis and folding of outer membrane proteins *in vitro* and *in vivo*: What have we learned to date? *Arch Biochem Biophys.* 2014; 564:265–280. [PubMed: 24613287]
2. Kim KH, Aulakh S, Paetzel M. The bacterial outer membrane beta-barrel assembly machinery. *Protein Sci.* 2012; 21:751–68. [PubMed: 22549918]
3. Hagan CL, Silhavy TJ, Kahne D. beta-Barrel membrane protein assembly by the Bam complex. *Annu Rev Biochem.* 2011; 80:189–210. [PubMed: 21370981]
4. Voulhoux R, Bos MP, Geurtsen J, Mols M, Tommassen J. Role of a highly conserved bacterial protein in outer membrane protein assembly. *Science.* 2003; 299:262–5. [PubMed: 12522254]
5. Ruiz N, Kahne D, Silhavy TJ. Advances in understanding bacterial outer-membrane biogenesis. *Nat Rev Microbiol.* 2006; 4:57–66. [PubMed: 16357861]
6. Sklar JG, Wu T, Kahne D, Silhavy TJ. Defining the roles of the periplasmic chaperones SurA, Skp and DegP in *Escherichia coli*. *Genes Dev.* 2007; 21:2473–84. [PubMed: 17908933]
7. Goemans C, Denoncin K, Collet JF. Folding mechanisms of periplasmic proteins. *Biochim Biophys Acta.* 2014; 1843:1517–28. [PubMed: 24239929]
8. Hartl FU, Bracher A, Hayer-Hartl M. Molecular chaperones in protein folding and proteostasis. *Nature.* 2011; 475:324–32. [PubMed: 21776078]
9. Walton TA, Sandoval CM, Fowler CA, Pardi A, Sousa MC. The cavity-chaperone Skp protects its substrate from aggregation but allows independent folding of substrate domains. *Proc Natl Acad Sci U S A.* 2009; 106:1772–7. [PubMed: 19181847]
10. Walton TA, Sousa MC. Crystal structure of Skp, a prefoldin-like chaperone that protects soluble and membrane proteins from aggregation. *Mol Cell.* 2004; 15:367–74. [PubMed: 15304217]

11. Korndorfer IP, Dommel MK, Skerra A. Structure of the periplasmic chaperone Skp suggests functional similarity with cytosolic chaperones despite differing architecture. *Nat Struct Mol Biol.* 2004; 11:1015–20. [PubMed: 15361861]
12. Jarchow S, Luck C, Gorg A, Skerra A. Identification of potential substrate proteins for the periplasmic *Escherichia coli* chaperone Skp. *Proteomics.* 2008; 8:4987–94. [PubMed: 19003857]
13. Qu J, Mayer C, Behrens S, Holst O, Kleinschmidt JH. The trimeric periplasmic chaperone Skp of *Escherichia coli* forms 1:1 complexes with outer membrane proteins via hydrophobic and electrostatic interactions. *J Mol Biol.* 2007; 374:91–105. [PubMed: 17928002]
14. Moon CP, Zaccai NR, Fleming PJ, Gessmann D, Fleming KG. Membrane protein thermodynamic stability may serve as the energy sink for sorting in the periplasm. *Proc Natl Acad Sci U S A.* 2013; 110:4285–90. [PubMed: 23440211]
15. Burmann BM, Wang C, Hiller S. Conformation and dynamics of the periplasmic membrane-protein-chaperone complexes OmpX-Skp and tOmpA-Skp. *Nat Struct Mol Biol.* 2013; 20:1265–72. [PubMed: 24077225]
16. Callon M, Burmann BM, Hiller S. Structural mapping of a chaperone-substrate interaction surface. *Angew Chem Int Ed Engl.* 2014; 53:5069–72. [PubMed: 24700611]
17. Bulieris PV, Behrens S, Holst O, Kleinschmidt JH. Folding and insertion of the outer membrane protein OmpA is assisted by the chaperone Skp and by lipopolysaccharide. *J Biol Chem.* 2003; 278:9092–9. [PubMed: 12509434]
18. Lyu ZX, Shao Q, Gao YQ, Zhao XS. Direct observation of the uptake of outer membrane proteins by the periplasmic chaperone Skp. *PLoS One.* 2012; 7:e46068. [PubMed: 23049938]
19. Kleinschmidt JH. Membrane protein folding on the example of outer membrane protein A of *Escherichia coli*. *Cell Mol Life Sci.* 2003; 60:1547–58. [PubMed: 14513830]
20. Bishop RE. The lipid A palmitoyltransferase PagP: molecular mechanisms and role in bacterial pathogenesis. *Mol Microbiol.* 2005; 57:900–12. [PubMed: 16091033]
21. Vandeputte-Rutten L, et al. Crystal structure of the outer membrane protease OmpT from *Escherichia coli* suggests a novel catalytic site. *EMBO J.* 2001; 20:5033–9. [PubMed: 11566868]
22. Yamashita E, Zhalnina MV, Zakharov SD, Sharma O, Cramer WA. Crystal structures of the OmpF porin: function in a colicin translocon. *EMBO J.* 2008; 27:2171–80. [PubMed: 18636093]
23. Noinaj N, Rollauer SE, Buchanan SK. The beta-barrel membrane protein insertase machinery from Gram-negative bacteria. *Curr Opin Struct Biol.* 2015; 31:35–42. [PubMed: 25796031]
24. Otzen DE, Andersen KK. Folding of outer membrane proteins. *Arch Biochem Biophys.* 2013; 531:34–43. [PubMed: 23131493]
25. Burgess NK, Dao TP, Stanley AM, Fleming KG. Beta-barrel proteins that reside in the *Escherichia coli* outer membrane *in vivo* demonstrate varied folding behavior *in vitro*. *J Biol Chem.* 2008; 283:26748–58. [PubMed: 18641391]
26. Heller KB. Apparent molecular weights of a heat-modifiable protein from the outer membrane of *Escherichia coli* in gels with different acrylamide concentrations. *J Bacteriol.* 1978; 134:1181–3. [PubMed: 350841]
27. McMorran LM, Bartlett AI, Huysmans GH, Radford SE, Brockwell DJ. Dissecting the effects of periplasmic chaperones on the *in vitro* folding of the outer membrane protein PagP. *J Mol Biol.* 2013; 425:3178–91. [PubMed: 23796519]
28. Ruotolo BT, Benesch JL, Sandercock AM, Hyung SJ, Robinson CV. Ion mobility-mass spectrometry analysis of large protein complexes. *Nat Protoc.* 2008; 3:1139–52. [PubMed: 18600219]
29. Hernandez H, Robinson CV. Determining the stoichiometry and interactions of macromolecular assemblies from mass spectrometry. *Nat Protoc.* 2007; 2:715–26. [PubMed: 17406634]
30. Ruotolo BT, et al. Evidence for macromolecular protein rings in the absence of bulk water. *Science.* 2005; 310:1658–61. [PubMed: 16293722]
31. Burmann BM, Holdbrook DA, Callon M, Bond PJ, Hiller S. Revisiting the interaction between the chaperone Skp and lipopolysaccharide. *Biophys J.* 2015; 108:1516–26. [PubMed: 25809264]
32. Sandlin CW, Zaccai NR, Fleming KG. Skp trimer formation is insensitive to salts in the physiological range. *Biochemistry.* 2015; 54:7059–7062. [PubMed: 26579730]



33. Bush MF, et al. Collision cross sections of proteins and their complexes: a calibration framework and database for gas-phase structural biology. *Anal Chem.* 2010; 82:9557–65. [PubMed: 20979392]
34. Ruotolo BT, Robinson CV. Aspects of native proteins are retained in vacuum. *Curr Opin Chem Biol.* 2006; 10:402–8. [PubMed: 16935553]
35. Zaccai NR, et al. Deuterium labeling together with contrast variation small-angle neutron scattering suggests how Skp captures and releases unfolded outer membrane proteins. *Methods Enzymol.* 2016; 566:159–210. [PubMed: 26791979]
36. Marklund EG, Degiacomi MT, Robinson CV, Baldwin AJ, Benesch JL. Collision cross sections for structural proteomics. *Structure.* 2015; 23:791–9. [PubMed: 25800554]
37. Siegert R, Leroux MR, Scheufler C, Hartl FU, Moarefi I. Structure of the molecular chaperone prefoldin: unique interaction of multiple coiled coil tentacles with unfolded proteins. *Cell.* 2000; 103:621–32. [PubMed: 11106732]
38. Schwalm J, Mahoney TF, Soltes GR, Silhavy TJ. Role for Skp in LptD assembly in *Escherichia coli*. *J Bacteriol.* 2013; 195:3734–42. [PubMed: 23772069]
39. Thoma J, Burmann BM, Hiller S, Muller DJ. Impact of holdase chaperones Skp and SurA on the folding of beta-barrel outer-membrane proteins. *Nat Struct Mol Biol.* 2015; 22:795–802. [PubMed: 26344570]
40. Burmann BM, Hiller S. Chaperones and chaperone-substrate complexes: Dynamic playgrounds for NMR spectroscopists. *Prog Nucl Magn Reson Spectrosc.* 2015; 86-87:41–64. [PubMed: 25919198]
41. Quan S, et al. Super Spy variants implicate flexibility in chaperone action. *Elife.* 2014; 3:e01584. [PubMed: 24497545]
42. Stirling PC, Bakhomou SF, Feigl AB, Leroux MR. Convergent evolution of clamp-like binding sites in diverse chaperones. *Nat Struct Mol Biol.* 2006; 13:865–70. [PubMed: 17021621]
43. Harms N, et al. The early interaction of the outer membrane protein phoe with the periplasmic chaperone Skp occurs at the cytoplasmic membrane. *J Biol Chem.* 2001; 276:18804–11. [PubMed: 11278858]
44. Robert V, et al. Assembly factor Omp85 recognizes its outer membrane protein substrates by a species-specific C-terminal motif. *PLoS Biol.* 2006; 4:e377. [PubMed: 17090219]
45. Estrada Mallarino L, et al. TtOmp85, a beta-barrel assembly protein, functions by barrel augmentation. *Biochemistry.* 2015; 54:844–52. [PubMed: 25537637]
46. Hagan CL, Wzorek JS, Kahne D. Inhibition of the beta-barrel assembly machine by a peptide that binds BamD. *Proc Natl Acad Sci U S A.* 2015; 112:2011–2016. [PubMed: 25646443]
47. Patel GJ, Kleinschmidt JH. The lipid bilayer-inserted membrane protein BamA of *Escherichia coli* facilitates insertion and folding of outer membrane protein A from its complex with Skp. *Biochemistry.* 2013; 52:3974–86. [PubMed: 23641708]
48. Fleming KG. A combined kinetic push and thermodynamic pull as driving forces for outer membrane protein sorting and folding in bacteria. *Philos Trans R Soc Lond B Biol Sci.* 2015; 370:20150026. [PubMed: 26370938]
49. Kim YE, Hipp MS, Bracher A, Hayer-Hartl M, Hartl FU. Molecular chaperone functions in protein folding and proteostasis. *Annu Rev Biochem.* 2013; 82:323–55. [PubMed: 23746257]
50. Arora A, Abildgaard F, Bushweller JH, Tamm LK. Structure of outer membrane protein A transmembrane domain by NMR spectroscopy. *Nat Struct Biol.* 2001; 8:334–8. [PubMed: 11276254]
51. Ahn VE, et al. A hydrocarbon ruler measures palmitate in the enzymatic acylation of endotoxin. *EMBO J.* 2004; 23:2931–41. [PubMed: 15272304]
52. Ni D, et al. Structural and functional analysis of the beta-barrel domain of BamA from *Escherichia coli*. *FASEB J.* 2014; 28:2677–85. [PubMed: 24619089]
53. Seshadri K, Garemyr R, Wallin E, von Heijne G, Elofsson A. Architecture of beta-barrel membrane proteins: analysis of trimeric porins. *Protein Sci.* 1998; 7:2026–32. [PubMed: 9761484]
54. Calabrese AN, Watkinson TG, Henderson PJ, Radford SE, Ashcroft AE. Amphipols outperform dodecylmaltoside micelles in stabilizing membrane protein structure in the gas phase. *Anal Chem.* 2015; 87:1118–26. [PubMed: 25495802]

55. Morgner N, Robinson CV. Massign: an assignment strategy for maximizing information from the mass spectra of heterogeneous protein assemblies. *Anal Chem.* 2012; 84:2939–48. [PubMed: 22409725]
56. Smith DP, et al. Deciphering drift time measurements from travelling wave ion mobility spectrometry-mass spectrometry studies. *Eur J Mass Spectrom.* 2009; 15:113–30.
57. Benesch JL, Ruotolo BT, Simmons DA, Robinson CV. Protein complexes in the gas phase: technology for structural genomics and proteomics. *Chem Rev.* 2007; 107:3544–67. [PubMed: 17649985]
58. Maier JA, et al. ff14SB: Improving the Accuracy of Protein Side Chain and Backbone Parameters from ff99SB. *J Chem Theory Comput.* 2015; 11:3696–713. [PubMed: 26574453]
59. Tsui V, Case DA. Theory and applications of the generalized born solvation model in macromolecular simulations. *Biopolymers.* 2000; 56:275–291. [PubMed: 11754341]
60. Weiser J, Shenkin PS, Still WC. Approximate atomic surfaces from linear combinations of pairwise overlaps (LCPO). *J Comput Chem.* 1999; 20:217–230.
61. Irobalieva RN, et al. Structural diversity of supercoiled DNA. *Nat Commun.* 2015; 6:8440. [PubMed: 26455586]

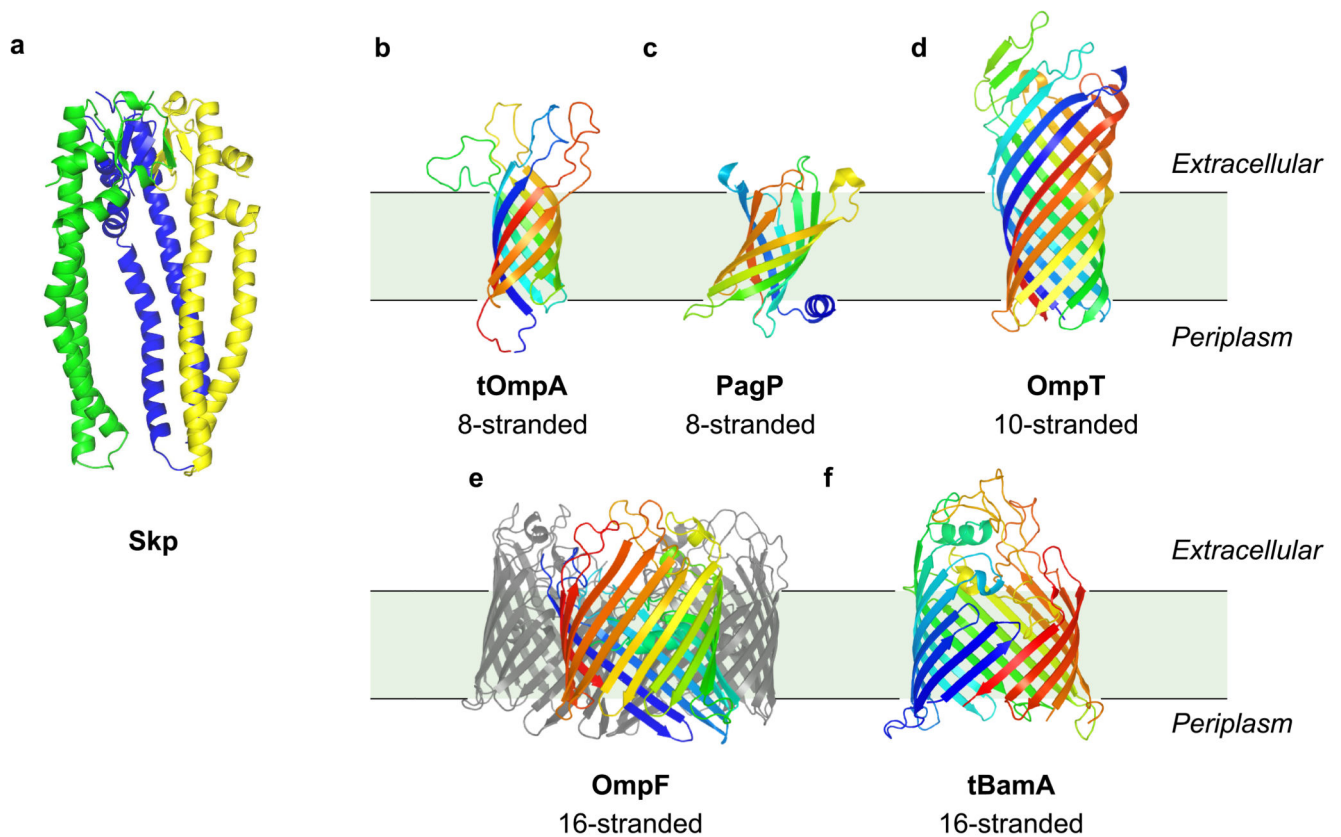
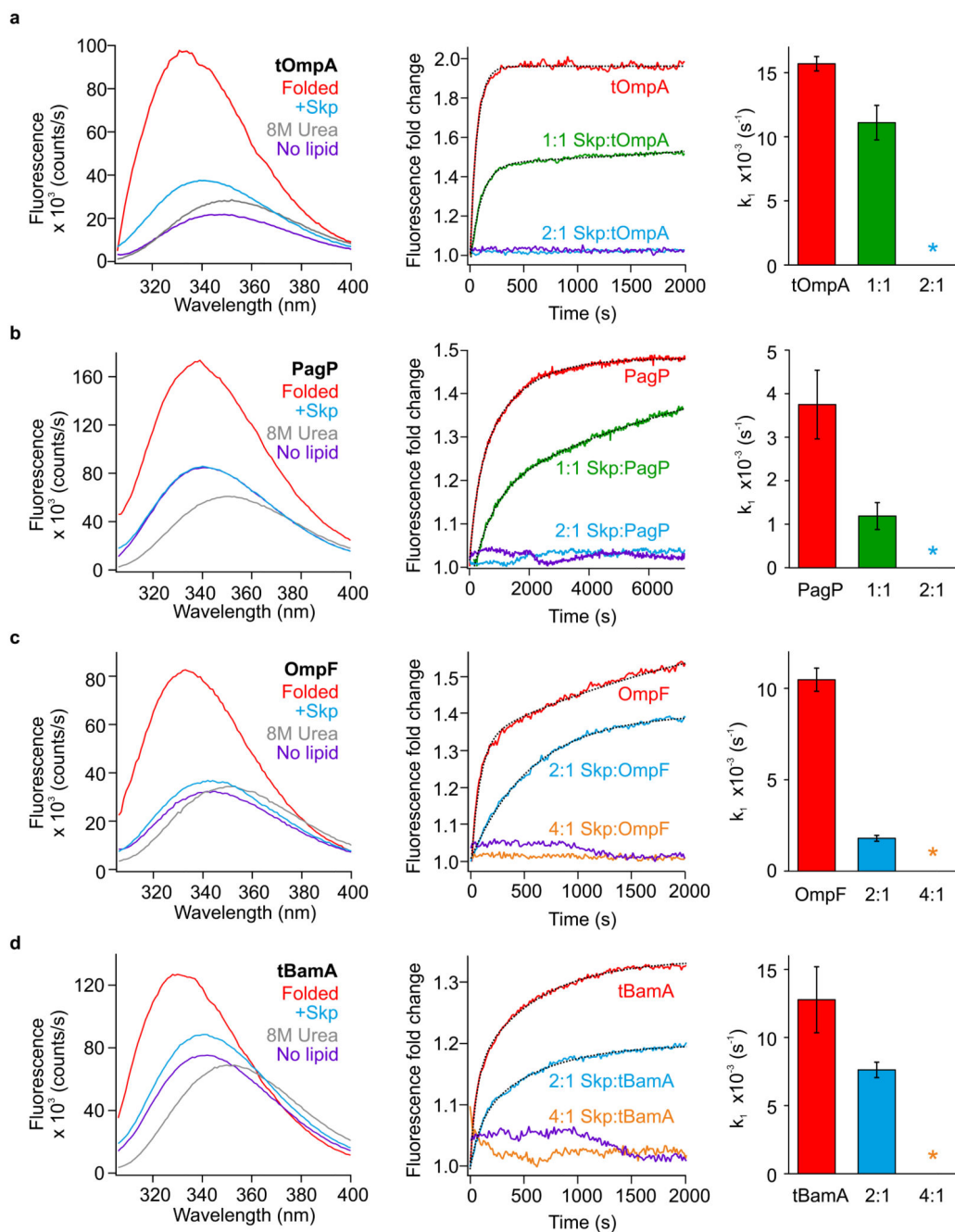


**Figure 1. Three-dimensional structures of Skp and the OMPs used in this study** (a) Skp (PDB 1U2M11), (b) tOmpA (PDB:1G9050), (c) PagP (PDB:1THQ51), (d) OmpT (PDB:1I7821), (e) OmpF (PDB:2ZFG22), and (f) tBamA (PDB 4N7552). All structures are to scale. OmpF is a functional trimer; for clarity only one subunit is colored and the other two are shown in grey. Residues missing from chains B and C in the Skp crystal structure were modelled from chain A (green). In (b)-(f) the OM is represented in pale green, and approximate positions of OMPs within the membrane are judged by the position of residues in the ‘aromatic girdles’ at either side of the membrane<sup>53</sup>.



(tOmpA and PagP, green lines, parts **(a)** and **(b)**), a 2:1 molar ratio (cyan lines, parts **(a)**–**(d)**), a 4:1 molar ratio (OmpF and tBamA, orange lines, parts **(c)** and **(d)**), or in the absence of lipids (purple lines). Single or double exponential fits to the data (see Supplementary Table 2) are shown as dotted lines. Rate constants for OMP folding in the absence or presence of Skp at the OMP:Skp ratio indicated (right). Where the data were best described by a double exponential fit, the rate constants for the second, slower, phase are not shown (see Supplementary Table 2 for full details). A star indicates a Skp:OMP ratio where folding did not occur on the timescale of these experiments. Data are shown as mean  $\pm$  standard deviation of three independent experiments using three separate liposome batches.

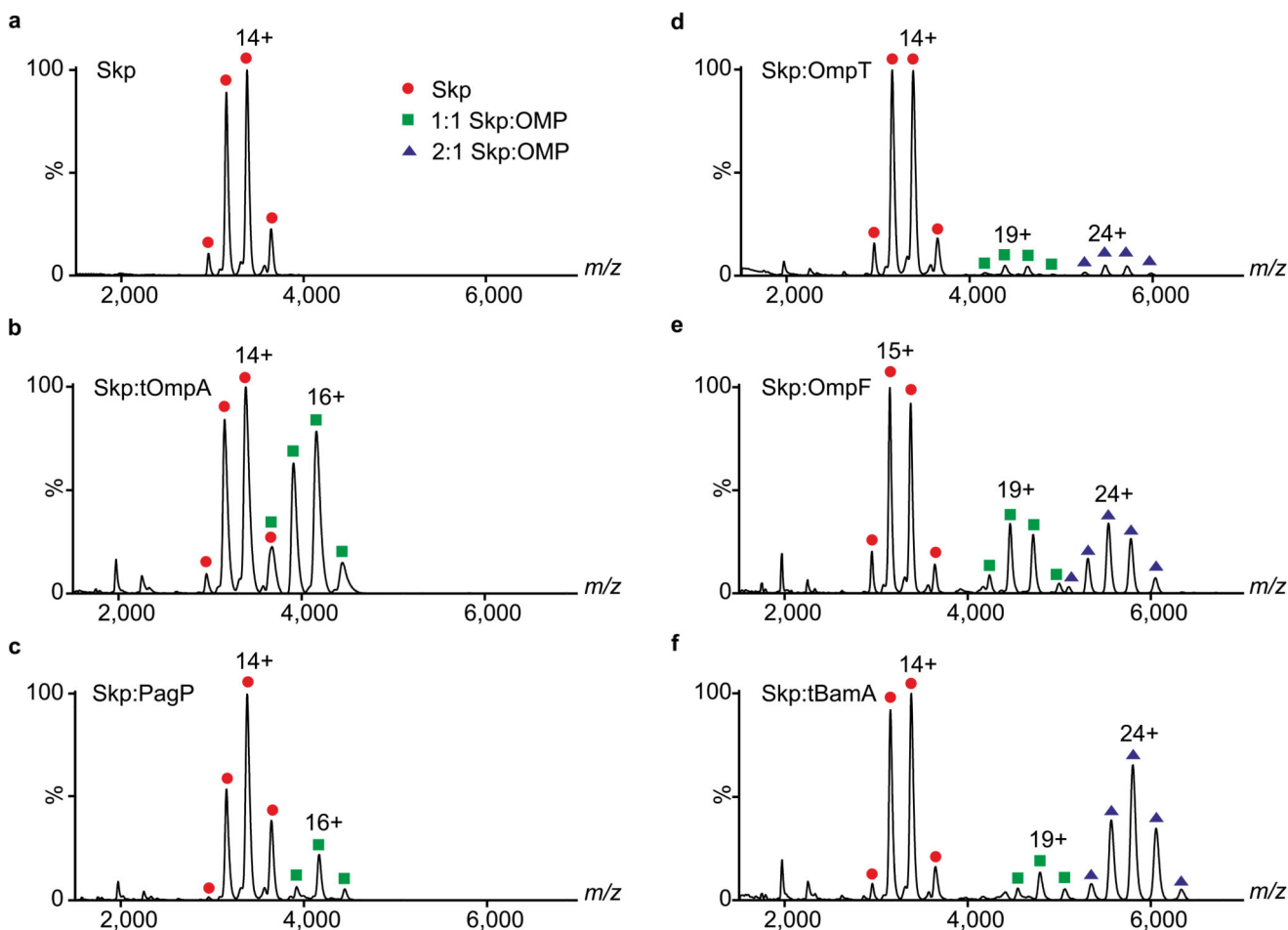


**Figure 3. Skp:OMP complexes have different stoichiometries.**

ESI mass spectra of (a) Skp (5  $\mu$ M) and Skp pre-incubated in the presence of 5  $\mu$ M (b) tOmpA, (c) PagP, (d) OmpT, (e) OmpF and (f) tBamA. Spectra are annotated with red circles (Skp), green squares (1:1 Skp:OMP) and blue triangles (2:1 Skp:OMP). The most abundant charge state is labelled for each distribution. Observed masses for the complexes are summarized in Supplementary Table 3. Complementary IMS data are displayed in Supplementary Fig. 3.

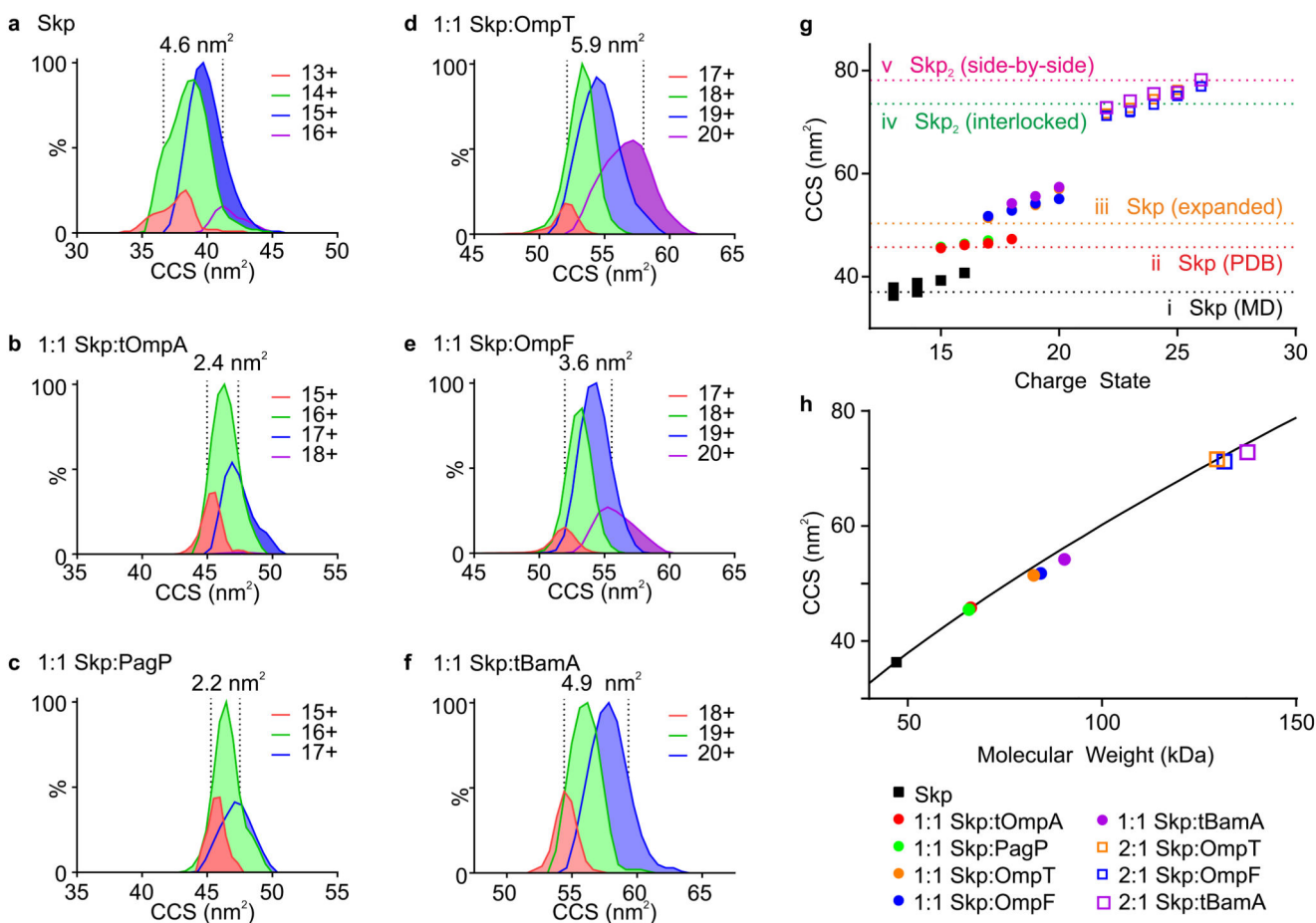


**Figure 4. Collision cross-section distributions of Skp and Skp:OMP complexes.**

CCS distributions (peak heights normalized to MS peak intensity) of (a) Skp and 1:1 Skp:OMP complexes with (b) tOmpA, (c) PagP, (d) OmpT, (e) OmpF and (f) tBamA. The width at half height (normalized for spectral intensity) for each distribution is indicated (dashed lines), as well as the charge states which are represented by each CCS distribution. (g) Plot of observed CCSs of the assemblies as a function of charge state (mean of three replicates shown, note that standard deviation values are smaller than the symbol size used): Skp, black squares; 1:1 Skp:tOmpA, red circles; 1:1 Skp:PagP, green circles; 1:1 Skp:OmpT, orange circles; 1:1 Skp:OmpF, blue circles; 1:1 Skp:tBamA, purple circles; 2:1 Skp:OmpT, orange open squares; 2:1 Skp:OmpF, blue open squares; 2:1 Skp:tBamA, purple open squares. Dashed lines indicate CCSs estimated from (i) the collapsed structure of Skp from the MD simulation (black) (Supplementary Fig. 7e), (ii) the crystal structure of Skp (red), (iii) a model 1:1 Skp:OMP complex with an expanded central cavity (orange), (iv) a model 2:1 Skp:OMP complex comprising two interlocking Skp molecules (green) and (v) a model (Skp)<sub>2</sub>:OMP complex arranged in a side-by-side fashion (pink) (Fig. 5). (h) Plot of the lowest measured CCS of each assembly as a function of molecular weight (symbols as in (g)). The line represents the expected CCSs for globular proteins with an amino acid density of 0.33 Da.Å<sup>-3</sup>.

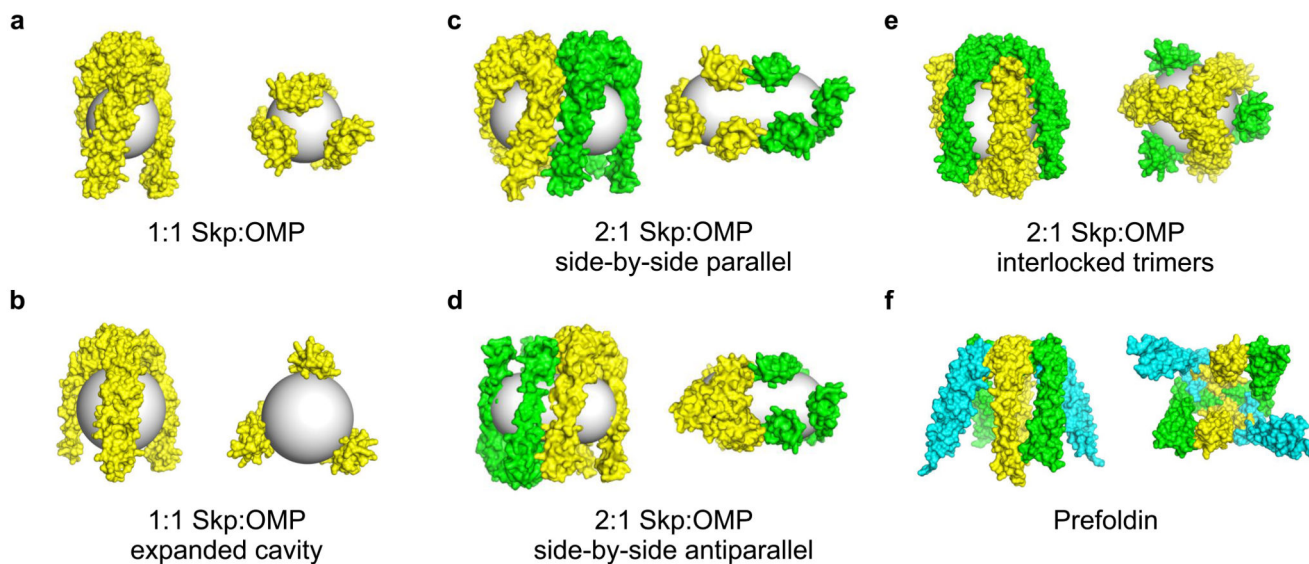


**Figure 5. Possible architectures of Skp:OMP complexes.**

Side (left) and bottom (right) view surface representations of models of **(a)** Skp (yellow) (based on the published crystal structure (PDB: 1U2M10) with missing residues modelled by molecular replacement), bound to an 8-stranded OMP represented by a grey sphere of radius 20 Å, **(b)** Skp with an expanded central cavity surrounding a 16-stranded OMP represented by a grey sphere of radius 25 Å, **(c,d)** 2:1 Skp:OMP structures (Skp colored in yellow and green) arranged side-by-side in a **(c)** parallel or **(d)** antiparallel arrangement, with the 16-stranded OMP substrate represented by a grey capsule with cylinder height of 37 Å and cap radii of 20 Å, **(e)** 2:1 Skp:OMP complex with an interlocked architecture with the 16-stranded OMP represented by a grey sphere of radius 25 Å, and **(f)** the hexameric eukaryotic chaperone prefoldin (PDB: 1FXK37), with chains A, B and C of the crystal structure shown in green, cyan and yellow, respectively.



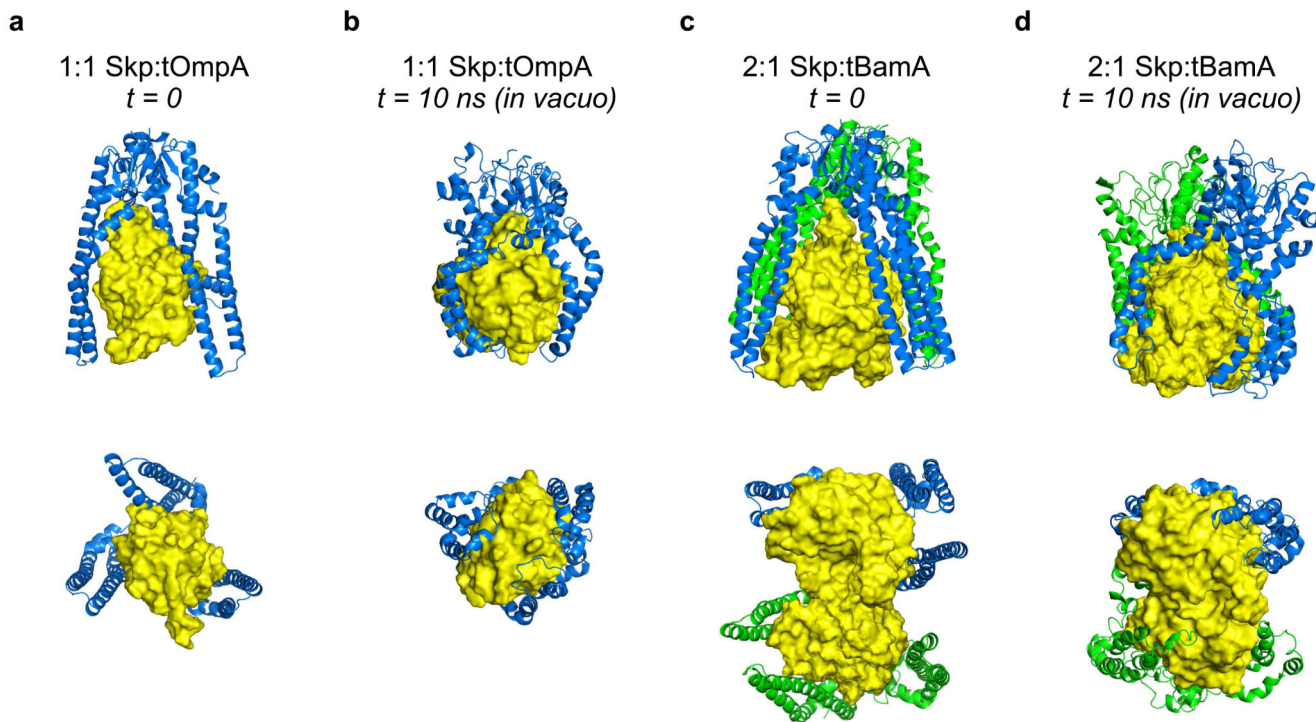


**Figure 6. *In vacuo* molecular dynamics simulations of 1:1 and 2:1 Skp-OMP complexes.**

(a) Starting model of a 1:1 Skp:tOmpA complex used for MD simulations (**Supplementary Data Set 4**), and (b) the structure obtained after 10 ns of *in vacuo* simulation (**Supplementary Data Set 5**). (c) Starting model of a 2:1 Skp:tBamA complex used for MD simulations, with the two copies of Skp arranged in a side-by-side parallel orientation (Fig. 5c) (**Supplementary Data Set 6**), and (d) the structure obtained after 10 ns of *in vacuo* simulation (**Supplementary Data Set 7**). Views from the side (top row) and bottom (bottom row) are shown. Skp (green/blue) is shown in cartoon representation. OMPs (yellow) are shown in surface representation. Representative structures are shown from three independent MD simulations, and CCS values in the text are the mean  $\pm$  standard deviation of three MD simulations.

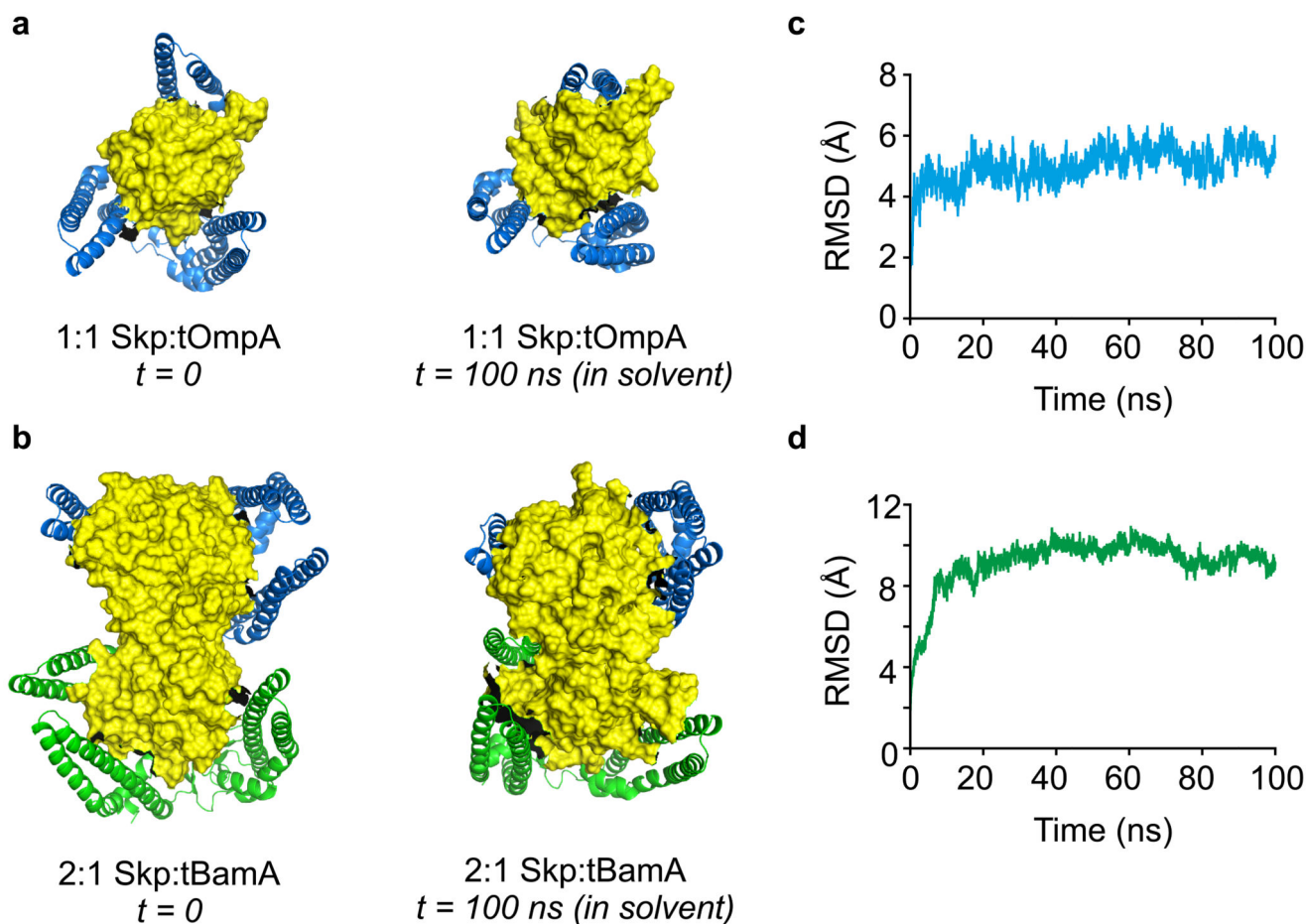


**Figure 7. Molecular dynamics simulations of 1:1 and 2:1 Skp:OMP complexes in explicit solvent.** (a) Starting model of a 1:1 Skp:tOmpA complex used for MD simulations (left) (**Supplementary Data Set 4**) and the structure obtained after 100 ns of simulation in explicit solvent (right) (**Supplementary Data Set 8**). (b) Starting model of a 2:1 Skp:tBamA complex used for MD simulations (left) (**Supplementary Data Set 6**), with the two copies of Skp arranged in a side-by-side parallel orientation (Fig. 5c), and the structure obtained after 100 ns of simulation in explicit solvent (right) (**Supplementary Data Set 9**). (c,d) Backbone RMSDs calculated for the 100 ns simulations of (c) 1:1 Skp:tOmpA, and (d) 2:1 Skp:tBamA in explicit solvent, demonstrating that the complexes are stable over this timescale. Representative structures are shown from three independent MD simulations, and CCS values in the text are the mean  $\pm$  standard deviation of three MD simulations.